JOURNAL OF CATALYSIS 116, 49–60 (1989)

Microcalorimetric Study of the Surface Structure of Graphite-Supported Iron/Rhodium Catalyst Particles

ROBERT R. GATTE[1] AND JONATHAN PHILLIPS[2]

Department of Chemical Engineering, Pennsylvania State University, 133 Fenske Laboratory, University Park, Pennsylvania 16802

Received August 23, 1988; revised October 18, 1988

The surface chemistry of graphite-supported iron/rhodium bimetallic catalyst particles was explored using a Calvet-type differential adsorption microcalorimeter of novel design and transmission electron microscopy. Oxygen was used as a probe gas to examine the changes in adsorption behavior as a function of oxidation and reduction treatments, while TEM provided clues about the particle microstructure. The results clearly indicate that the two metals segregate locally on calcination above 200°C and do not form an alloy phase after a subsequent low-temperature (100°C) reduction. There is also evidence to support the conclusion that the 200°C calcination treatments leads to iron enrichment of the particle surface, which is also retained after the subsequent 100°C reduction. This study further supports a model presented previously (R. R. Gatte and J. Phillips, *J. Phys. Chem.* **91**, 5961, 1987) of the structural dynamics of graphite-supported Fe/Rh catalyst particles.

INTRODUCTION

In a recent article (*1*), a model of the structural dynamics of a graphite-supported iron/rhodium bimetallic catalyst system was proposed. Using Mössbauer spectroscopy, X-ray diffraction, and transmission electron microscopy, a new model of the dynamic phase behavior of supported Fe/Rh particles was established that differed from previous models (*2–6*) developed for similar particles supported on refractory oxides. Specifically, it was shown that localized segregation of the iron and rhodium (within a single particle) could be induced by calcination of the catalyst above 200°C. The independent iron oxide and rhodium oxide phases formed by this treatment could then be independently reduced to zones of zerovalent bcc iron and fcc rhodium by hydrogen reduction at temperatures below 100°C. In contrast, alloy formation occurred when the reduction temperature was raised to 400°C, resulting in uniform particles of bcc FeRh alloy.

The previous study (*1*) resolved several questions about the bulk behavior of supported iron/noble metal bimetallic particles, but did not address the question of surface chemistry. The work presented in this paper is intended to examine the structure of the *surface* of the bimetallic Fe/Rh particles following various oxidation and reduction treatments. To accomplish this, the adsorption of oxygen was studied using a differential adsorption microcalorimeter of the Tian–Calvet heat-flow design (*17–22*). Oxygen was chosen as the adsorbate because the heat and stoichiometry of adsorption of oxygen are significantly higher on iron than on rhodium (*21–23*). The calorimetric "signatures" of the two metals are therefore distinct and unmistakable. Hence, a comparison of the differential heat of oxygen adsorption on the bimetallic with that on the two monometallics provides information that readily allows determination of the relative contributions to the total adsorption of each of the individual metal components.

[1] Present address: W. R. Grace & Company, 7379 Route 32, Columbia, MD 21044.

[2] To whom correspondence should be addressed.

0021-9517/89 $3.00

The calorimetric and microscopic data collected in this work provide further evidence in support of the localized segregation model discussed previously (*1*). Specifically, it was found that, following calcination of the alloyed catalyst at 200°C, the adsorption behavior (both the heat profile and the total uptake) was directly dependent on the subsequent reduction temperature prior to adsorption. High-temperature (400°C) reduction/alloying produced a surface that acted like neither iron nor rhodium. The adsorption behavior of this alloy phase implied that the surface was composed of an ordered array of Fe and Rh atoms (i.e., a true ordered-alloy surface). In contrast, 200°C calcination followed by reduction at 100°C resulted in a surface which was probably iron enriched. That is, the heats of adsorption and the adsorption stoichiometry were close to those of pure iron.

EXPERIMENTAL

Catalyst preparation. The catalyst preparation scheme has been described in detail elsewhere (*1*). Briefly, the sample was prepared via impregnation of GTA-grade Grafoil (Union Carbide Corp.) with a benzene solution of μ-(η-(cycloheptatrienyl))-tricarbonyl-iron-cyclooctadiene-rhodium (*24*). The preparation was conducted under a nitrogen atmosphere, and a final loading of approximately 5.4% total metal (by weight) was achieved. The sample was loaded into the microcalorimeter pretreatment reactor (*19, 21*) and reduced in hydrogen at 400°C for 6 h to decompose the precursor and reduce/alloy the metals. A subsequent XRD pattern indicated that the only species present in the sample was the bcc alloy phase, as was expected for the 50/50 Fe/Rh atomic ratio (*1, 25–28*).

Differential adsorption microcalorimetry. The principles of Calvet heat-flow calorimeters in general as well as the design of the microcalorimeter used for this study have been described in detail elsewhere (*17–22*). The present system allows (i) *in situ* sample pretreatment prior to adsorption, (ii) accurate volumetric measurements, (iii) determination of the real differential heat of adsorption versus uptake, and (iv) collection of qualitative kinetic information as to the rates of adsorption and subsequent heat generation. In short, it is designed to allow the collection of typical static chemisorption data with the added capabilities of a heat-flow microcalorimeter.

The catalyst typically was pretreated as follows: (i) hydrogen reduction at the temperature of interest (30, 100, or 400°C); (ii) evacuation (1×10^{-6} Torr) at the same temperature to remove adsorbed hydrogen; (iii) cooldown, transfer to calorimeter cell, and equilibration at 30°C, all while maintaining dynamic vacuum (1×10^{-6} Torr). Chemisorption experiments were then conducted by sequentially exposing the sample to oxygen (approximately 0.6 μmol per dose) initially at 1.0 Torr, and following the resulting heat evolution and pressure decrease (i.e., adsorption dynamics) until equilibrium was reestablished. Some characteristic thermograms are reproduced in Fig. 1a. The heat of adsorption of each dose is determined from the area under the corresponding heat peak (*17–22*). Figure 1b presents some typical pressure–response curves. As described elsewhere (*21*), the pressure is measured in the dosing volume by Baratron capacitance manometers. A qualitative parameter that is representative of the rate of adsorption has been defined on the basis of the shape of the curves shown in Fig. 1b. This *normalized adsorption parameter* is used to obtain qualitative information about the changes that occur in the adsorption rate as a function of coverage. The parameter represents the time it takes for the pressure to come to within 10% of its equilibrium value, normalized by the first point of the data set.

Transmission electron microscopy. TEM micrographs of the sample were collected after the various treatments described below. Small flakes of the catalyst were supported on copper grids and examined in a

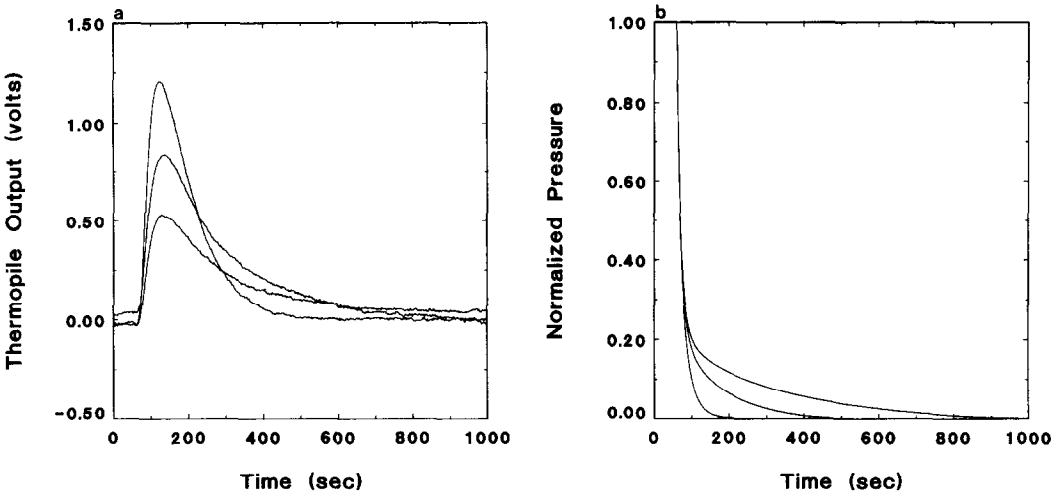

FIG. 1. Typical raw calorimeter data. (a) Characteristic thermograms: The heat evolved during each dose is determined from the integrated area under the peaks. (b) Characteristic pressure–response curves: The rate of adsorption is qualitatively estimated from the time it takes the pressure to come to within 10% of its equilibrium value. In both cases, the gas dose is admitted into the sample cell after 60 s of baseline collection.

Philips Model 420 STEM unit, equipped with EDX. Particle size distributions were obtained by counting a statistically significant number of particles (over 800). Dispersions were estimated assuming hemispherically shaped particles, using the ideas of Matyi *et al.* (*29*).

RESULTS

High-temperature reduction. The 5.4% FeRh/Grafoil catalyst sample was initially treated in hydrogen at 400°C for 6 h, followed by evacuation at 400°C (1×10^{-6} Torr) and subsequent cooldown and transfer into the calorimeter cell as described above. Previous studies (*1*) by Mössbauer spectroscopy and X-ray diffraction indicated that this treatment procedure resulted in the formation of uniform particle of bcc FeRh alloy. This was confirmed by XRD (see above) and by the TEM micrograph shown in Fig. 2, which depicts some representative particles following this high-temperature reduction. The metal crystallites appear to be both uniform and three dimensional. Elemental analysis by EDX verified that their composition was approximately 50/50 Fe/Rh. The TEM was also used to generate a particle size distribution (Fig. 3), from which an effective metal surface area or dispersion was calculated (as described above). Using this approach, a dispersion of approximately 7.5% was estimated for the sample. This number was used to estimate the oxygen atom : surface metal atom ($O : M_s$) ratios presented in Table 1.

Differential heat of adsorption data are given in Fig. 4 for 30°C oxygen adsorption on these bcc FeRh alloy particles. Data from two such experiments are presented to demonstrate repeatability. (In fact, all adsorption data shown in this study were repeatably obtained. Hereafter, for clarity, only a single data set is shown after each treatment.) In Fig. 4, the heat is seen to fall monotonically with increasing coverage, from an initial high value near 130 kcal/g mol O_2 adsorbed to values near 50 kcal/g mol O_2 adsorbed, until the surface was completely saturated and only physical adsorption was occurring. The separation into the two regions was made on the basis of the changes observed in the adsorption dynamics, as indicated by the rate of gas up-

FIG. 2. TEM micrograph taken after 400°C hydrogen treatment of the FeRh/Grafoil sample.

take. In Region I, the gas was adsorbed immediately on expansion into the sample cell, and the heat evolved in a sharp peak. However, in Region II, the rate of oxygen uptake slowed with each successive dose until the surface was fully passivated. Similar changes in adsorption dynamics also were seen for both of the monometallic samples (*21, 22*).

A qualitative comparison between the adsorption data of the bimetallic alloy and those of similarly prepared Grafoil-supported Fe and Rh monometallic catalysts is given in Fig. 5. In this figure, the data have been normalized so that the total amount of chemisorbed oxygen in each case corresponds to a fractional coverage of 1.0. The data show that oxygen adsorption on iron is a steady, high-heat process through a coverage of approximately 0.75, at which point the adsorption process slows significantly, and the heats rapidly fall off until the surface is completely passivated, and only physical adsorption is occurring (*21*). In contrast, the heat of adsorption of oxygen on rhodium is seen to steadily decrease from the start. This decrease becomes more rapid after a fractional coverage of approximately 0.6, at which point the adsorption slows dramatically with each successive dose, again until the physical adsorption point is reached (*22*). The heats of oxygen adsorption on the alloyed bimetallic catalyst (bcc FeRh alloy) fall between the two monometallic extremes throughout the coverage range. The data in Fig. 4 are probably

TABLE 1

Differential Adsorption Data for the Various Grafoil-Supported Systems Described in the Text

Catalyst/treatment	Integral Q_{ads} (kcal/g mol O_2)	Uptake (mol O_2/mol M)	Approximate Fe_s composition[a] (mol%)	Approximate $O:M_s$ ratio[b]
α-Fe	130	0.068	100	3.3
τ-Rh	67	0.046	0	0.7
α-FeRh (400°C H_2)	98	0.035	50	1.0
Fe/Rh (200°C air/30°C H_2)	105	0.007	60	0.2
Fe/Rh (200°C air/100°C H_2)	122	0.062	85	1.7
Fe/Rh (second 30°C H_2)	100	0.016	50	0.4

[a] Estimated via an energy/material balance, using the measured integral heats of adsorption for the species present.

[b] Surface area (dispersion) estimated from the measured particle size distribution (Fig. 3), assuming hemispherical particles.

the result of adsorption on an alloy surface. The initial iron-like heats are reasonable, since oxygen is expected to preferentially adsorb on iron sites at low coverage due to the high heats associated with Fe–O bond formation. As coverage increased, the heats fall off as the rhodium sites become progressively more important. This model also explains why the oxygen atom/surface atom stoichiometry is ~1.0 (Table 1). That is, an alloy would not show multilayer oxidation. The integral heat of adsorption (98 kcal/g mol O_2 adsorbed) is almost exactly the average of those of the two monometallics (130 kcal/g mol O_2 for Fe; 67 kcal/g mol O_2 for Rh). This suggests that the fractional composition of the surface is 50/50 Fe/Rh as might be expected for a true alloy surface. This model is also consistent with models of oxidation of bimetallic alloys consisting of iron and a noble metal (*30*).

Oxidation/30°C reduction. Following the experiments presented above, the sample

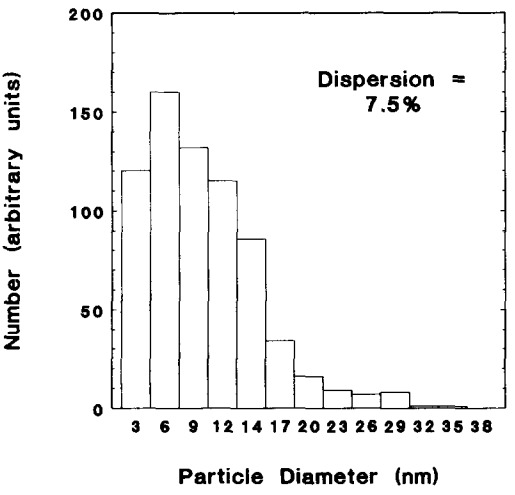

FIG. 3. Particle size distribution estimated by counting particles from TEM micrographs. Approximately 800 particles were counted to generate the histogram. The dispersion was calculated using the ideas of Matyi *et al.* (*29*).

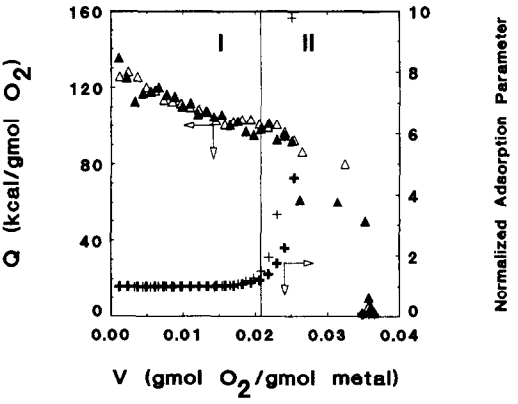

FIG. 4. Differential heat and rate of oxygen adsorption (at 30°C) on alloyed (400°C reduced) FeRh/Grafoil sample. The data from two separate experiments are presented to demonstrate repeatability.

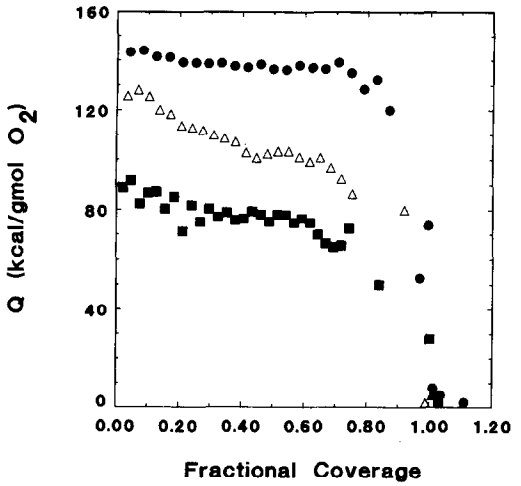

FIG. 5. Comparison between differential heat of oxygen adsorption on Fe/Grafoil (closed circles), Rh/Grafoil (closed squares), and FeRh/Grafoil (open triangles). The fractional coverage is obtained by normalizing the data by the total amount of irreversibly adsorbed oxygen for each sample.

was treated in air at 200°C. This treatment was shown in past work to induce segregation of the two metal species into localized "zones" of Fe oxide and Rh oxide (*1*). Following the oxidation treatment, the particles appear as nonuniform distributions of fields of light and dark, arising from localized density differences within single bimetallic particles (Fig. 6). EDX verified that the particles maintained the original 50/50 metal composition. However, the structure has been clearly altered by the oxidation.

Figure 7 presents the data from oxygen adsorption on the catalyst following various low-temperature hydrogen reductions of the previously segregated particles. The sample was first treated in hydrogen at 30°C, a treatment that has been previously shown to induce some degree of reduction of both the iron and rhodium in the sample (*1–10*). The subsequent oxygen adsorption data are represented by the closed circles in Fig. 7. As can be seen, the heat initially begins at approximately 140 kcal/g mol O_2 adsorbed, close to that expected for monometallic iron, but falls almost immediately to much lower values. Also, the uptake is substantially smaller than that of the alloy particles, showing that not all of the surface has been reduced by the 30°C hydrogen treatment. The integral heat of adsorption for this run (see Table 1) is roughly the same as that of the alloy phase (approximately 105 kcal/g mol O_2 versus 98 kcal/g mol O_2 for the alloy).

Oxidation/100°C reduction. The adsorption behavior of the sample after 200°C oxidation and subsequent 100°C reduction is dramatically different. This is shown by the closed squares in Figs. 7 and 8. First, the heats are higher than after 30°C reduction (approximately 140 kcal/g mol O_2 adsorbed), and remain high to a much higher coverage. In addition, the rates of adsorption (as measured by the normalized adsorption parameter in Fig. 8) are constant through a fractional coverage above 0.7, at which point the process dynamics change, and the rate falls with each successive dose. This behavior is much more iron-like than that of the alloy (as seen in Fig. 4), possibly signifying that the surface is enriched in iron following the oxidation treatment. This suggestion is further supported by the substantially higher integral heat of adsorption (122 kcal/g mol O_2) seen for this sample (Table 1). Second, the total coverage is nearly twice that of the alloy phase. This can be explained by either an increase in the metal surface area, or a change in the adsorption stoichiometry on the surface composed of two segregated metals versus that on the uniform alloy surface. This will be explored in more detail below.

TEM micrographs of the sample following this 100°C reduction (Fig. 9) showed nonuniformity similar to that of the oxidized particles (Fig. 6). These internal variations are interpreted as resulting from internal composition differences, similar to those of the fully oxidized particles. However, since both phases are metallic in Fig. 9, the density variations are not as clear as they are in Fig. 6, in which both phases are oxides.

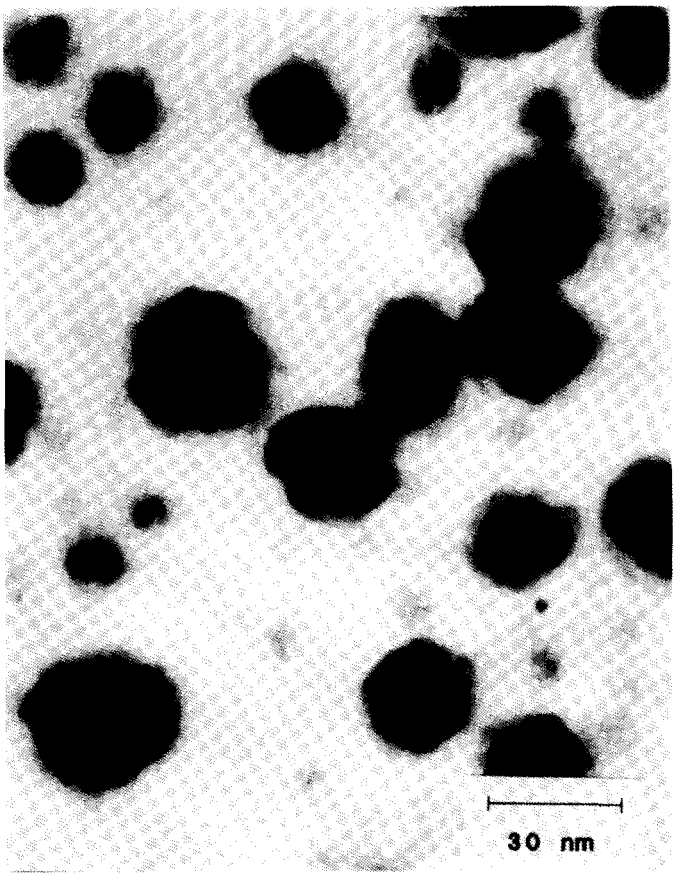

FIG. 6. TEM micrograph taken after 200°C oxidation of the FeRh/Grafoil sample.

Rereduction at 30°C. The sample was subsequently reduced in hydrogen at 30°C again, in an attempt to clean the previously adsorbed oxygen from the surface of the metal particles. The resulting heats of oxygen adsorption are shown as the closed diamonds in Fig. 7. The data show that, once again, the heats begin at values characteristic of monometallic iron, but drop off quickly. The ultimate uptake is only a quarter of that measured after the 100°C reduction, which indicates that the surface is only partially reduced during the 30°C reduction treatment. This is an apparent contradiction to the conclusions reached on the basis of Mössbauer spectroscopy (*1*), which indicated that the same series of treatments (i.e., 200°C oxidation, 100°C reduction, 30°C oxidation, 30°C reduction) led to the formation of particles which were reduced to a substantial extent. The Mössbauer singlet resulting from the 100°C reduction, which was partially oxidized on 30°C air exposure, returned in its entirety when the sample was subsequently treated in hydrogen at 30°C. This apparent discrepancy will be pursued further in the next section.

Finally, the integral heat of adsorption for this case is again close to 100 kcal/g mol O_2 adsorbed. This is in accordance with the previous 30°C reduction (the closed circles of Fig. 7). However, the uptake measurements are different for the two room-temperature reduction experiments, as shown in Table 1.

The sample was finally treated in hydro-

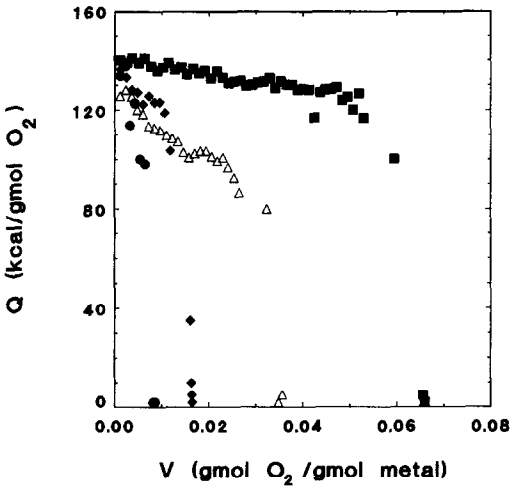

FIG. 7. Differential heat of oxygen adsorption (at 30°C) on the FeRh/Grafoil sample after 200°C oxidation and 30°C reduction (closed circles), 100°C reduction (closed squares), and a subsequent 30°C reduction (closed diamonds). The data from the bcc FeRh alloy (open triangles) are given for comparison.

gen at 400°C to verify that the alloy phase could be repeatedly formed. The resulting differential heat data were identical to those shown in Fig. 4, except that the ultimate uptake had decreased by approximately 20%. This is the result of particle sintering, which increased the average particle size. Despite the increase in particle size, however, the particle morphology clearly returned to that of the bcc FeRh bimetallic.

DISCUSSION

On the basis of the heat data and TEM micrographs presented above, and the Mössbauer and XRD data presented in a previous article (*1*), a model of the dynamics of the bimetallic particle morphology as a function of oxidation and reduction treatment can be proposed. A schematic diagram of this model is presented in Fig. 10.

The first state of the catalyst is the bcc FeRh alloy, which results from high-temperature (400°C) hydrogen treatment. According to structural information from Mössbauer spectroscopy, XRD, and TEM, the metal particles exist primarily as single, three-dimensional crystals of ordered bcc FeRh alloy. This is represented schematically by Fig. 10a. On the basis of the heat of adsorption data presented above, it appears that the surface of these alloy particles is possibly a true ordered alloy surface. This is inferred from several aspects of the data. First, the differential heat data fall monotonically between the two monometallic extremes. Second, the integral heat of adsorption is consistent with a surface which is 50/50/ Fe/Rh. Finally, the ultimate oxygen uptake on the alloy catalyst corresponds roughly to an $O:M_S$ ratio of 1.0. In other words, the oxygen adsorption proceeds to monolayer coverage. This is drastically different from the behavior of monometallic iron, which exhibits an $O:Fe_s$ ratio higher than 3.0 (*21, 35*). In sum, the adsorption behavior is consistent with that anticipated for a 50/50 alloy surface and clearly is inconsistent with a surface significantly enriched by either of the constituent metals.

The second state of the catalyst is shown schematically in Fig. 10b. This state consists of segregated, immiscible monometallic oxides (Fe_2O_3 and Rh_2O_3) formed by calcination (oxidation) at temperatures above 200°C. According to Kubaschewski and Hopkins (*30*), the oxidation of bulk alloy crystals containing a noble metal (Rh) and a

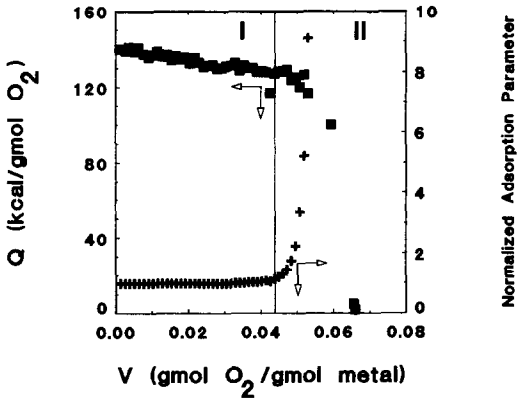

FIG. 8. Differential heat and rate of oxygen adsorption on the FeRh/Grafoil sample after 200°C oxidation and 100°C reduction.

FIG. 9. TEM micrograph taken after 100°C reduction of the previously oxidized FeRh/Grafoil sample.

base (Fe) proceeds through stages which can induce the segregation of the two metals into separate oxide phases. Initially the base metal will be preferentially "attacked" by oxygen atoms, and will segregate to form an oxide layer on the surface of the sample. The mechanism for the growth of this oxide film is by diffusion of base metal ions to the surface. Eventually, the noble metal will also be oxidized, forming a subfilm beneath the surface film. Stresses, built up by changes in the density of the particles due to oxidation, will cause the oxide films to crack and break into "islands" which will become dispersed within each other. The resulting oxidized particles will appear similar to that shown in Fig. 10b. The surface will be enriched in the base metal oxide (Fe_2O_3), while the noble metal oxide (Rh_2O_3) will be dispersed primarily in the interior of the particles (*30*).

The Kubaschewski oxidation model apparently explains the "postoxidation" data obtained in both the present and preceding studies (*1*). First, the structural information from MES and XRD indicate that the metals have segregated into separate oxide species. Second, the TEM micrographs (Fig. 6) clearly show that the particles have a morphology completely altered from that of the alloy phase. The particles exhibit internal density variations, and no longer ap-

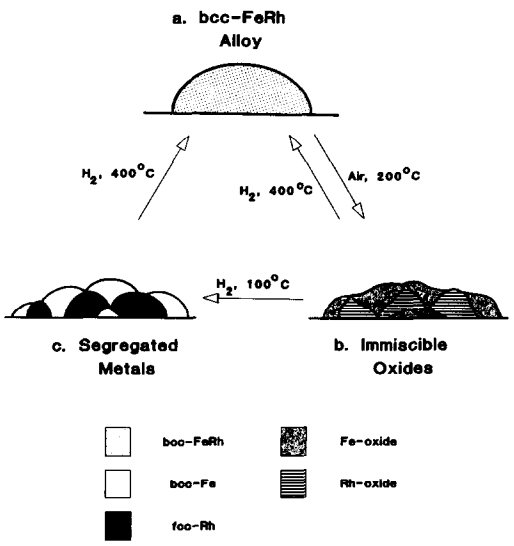

FIG. 10. Schematic model of the proposed particle dynamics for the FeRh/Grafoil sample. (a) Uniform bcc FeRh alloy formed during 400°C reduction. (b) Segregated immiscible oxides (Fe_2O_3 and Rh_2O_3) formed during 200°C oxidation, showing the iron enrichment of the surface. (c) Segregated metals formed during 100°C reduction of the previously oxidized sample, again showing the iron enrichment of the surface.

pear as single uniform crystallites. Third, the differential heat data collected after 200°C oxidation/100°C reduction (Figs. 7 and 8) clearly indicate that the surface has been enriched in iron. This fits the oxidation model if it is assumed that the enrichment takes place during the oxidation step, and that little further metal atom diffusion occurs during the subsequent 100°C reduction. There is also precedent for the proposed model in the catalyst literature.

It has been previously shown that the surface of Pt–Rh alloy particles becomes enriched with a Rh oxide layer following oxidation. The Rh enrichment remains following reduction (*31, 32*). Similarly, an iron oxide surface layer forms following the oxidation of Fe–Mn particles (*33*). These models differ from the present in that they suppose the formation of uniform, segregated spherical shells which are enriched with one metal rather than segregation into single metal localized zones (not shells).

Upon room-temperature (30°C) hydrogen treatment of the oxidized sample it is apparent that a small part of the particle surface has been reduced. Indeed, the oxygen uptake given in Table 1 is only about 20% of that seen on the alloy surface. In addition, the integrated heat of oxygen adsorption (105 kcal/g mol O_2) indicates that both Fe and Rh atoms are responsible for the adsorption (see Table 1). The fact that the surface has been reduced at all indicates that at least part of it is composed of rhodium atoms because it is well known (*1–16*) that reduction of monometallic iron catalysts requires high temperatures (400°C). The usual proposed mechanism for this enhanced reduction of iron at room temperature is that of hydrogen atom spillover from Rh surface sites to neighboring Fe sites (*2, 12*). That is, it is suggested that the Rh atoms act as active sites on which hydrogen molecules are dissociated into atoms, which are then free to react and reduce.

The spillover model does not appear to fully explain many of the observations made in this study. For example, the apparent contradiction between the MES and calorimeter results obtained following the sequence 200°C oxidation/100°C reduction/30°C oxidation/30°C reduction is not explained by this model. MES shows virtually complete reduction following this sequence, while calorimetry indicates only a very limited amount of surface iron reduction (see Results). If spillover were the mechanism of iron surface reduction, then most of the surface iron would be reduced after the above sequence.

An alternative to the hydrogen spillover model (the noble metal pump model), which is consistent with all of the MES and calorimetry results, is presented below. In a hydrogen atmosphere, metallic rhodium reduces neighboring iron oxide on the basis of an oxygen chemical potential gradient, and the oxygen diffusion which results (*34*). That is, oxygen diffuses from the iron oxide into the rhodium; it then readily diffuses to the rhodium surface where is is "pumped"

away by adsorbed hydrogen. At 30°C, due to limited ion mobility [well established in the literature (*35, 36*)], only two or three layers of oxygen immediately adjacent to the rhodium are removed from the iron. At 100°C the ions are more mobile [again well established in the literature (*36*)], such that all of the oxygen is pumped away, and the iron is fully reduced. Thus, in the sequence described above, all of the iron will be reduced after the 100°C hydrogen treatment (MES and calorimetry agree). Only the surface, as shown using calorimetry, will be reoxidized at 30°C, having, as found (*1*), only a small effect on the MES spectrum as MES is fundamentally a "bulk" technique. Finally, during hydrogen treatment at 30°C only iron (in the bulk and at the surface) immediately adjacent to rhodium will be reduced. This will allow for very limited oxygen uptake on iron, as found. Although this model explains all the results (see Fig. 7, for example), it must be considered speculative.

Upon reduction of the particles at 100°C, the third distinct state of the metal particles is formed. This is a state of segregated zero-valent metals (Fig. 10c). This is supported by (i) Mössbauer spectroscopy, which indicates the existence of a zero-valent iron phase (*1*); (ii) XRD, which shows the existence of fcc rhodium (*1*); (iii) TEM (Fig. 9), which shows that the particles retain their internal density variations despite the high degree of reduction; and (iv) the differential and integral heat data (Figs. 7 and 8 and Table 1), which indicate that the majority species on the surface is iron. It is proposed that this relatively low-temperature reduction is sufficient to reduce the two oxide species into the zero-valent state, via the mechanism described above, but that inadequate thermal energy is available for interdiffusion of the two metals to reform the bcc FeRh alloy. Hence, the surface exists primarily as reduced iron, with small patches of rhodium.

The increased uptake of the sample after the 100°C reduction (nearly twice that of the alloy) is attributed primarily to the stoichiometry of oxygen adsorption on iron which is significantly higher than 1.0. In fact, it has been reported that the $O:Fe_s$ ratio is higher than 3.0 for room-temperature oxygen adsorption on evaporated iron films (*35*) and supported iron particles (*21*). Indeed, simple calculations indicate that, if 85% of the adsorption is due to iron atoms (as indicated by the approximate surface composition shown in Table 1), then a change in stoichiometry to 2 : 1 $O:Fe_s$ can account for the increased uptake. Another possibility which cannot be discounted, however, is that some of the increase in oxygen uptake on the segregated metal particles can be attributed to an increase in particle surface are due to particle cracking during the oxidation and subsequent reduction (*37, 38*).

The structural model proposed in Fig. 10 is valid for the Grafoil-supported bimetallic system examined in the present work. An extension of the model to other systems cannot be made directly. For example, the use of oxidic substrates (SiO_2, Al_2O_3, etc.) introduces the possibility of significant support interactions which will alter the particle morphology (*39*), possibly by segregation of iron to the particle–support interface (*2*).

In sum, in this study the model of dynamic phase behavior of Fe/Rh catalyst particles presented previously (*1*) was reconfirmed. In addition, it was shown using a heat flow calorimeter of novel design that the iron zones make up the majority, but not all, of the surface following segregation. This study and others (*1, 31–33*) demonstrate the variety of catalytic surfaces which can be produced through appropriate pretreatment of bimetallic systems.

ACKNOWLEDGMENTS

The authors gratefully acknowledge the support of the National Science Foundation (Grant CPE-8305937) and the Pennsylvania State University Engineering School Equipment Program (Ben Franklin Partnership for Advanced Technology).

REFERENCES

1. Gatte, R. R., and Phillips, J., *J. Phys. Chem.* **91,** 5961 (1987).
2. Niemantsverdriet, J. W., and van der Kraan, A. M., *in* "Industrial Applications of the Mössbauer Effect" (G. J. Long and J. G. Stevens, Eds.), p. 609. Plenum, New York, 1986.
3. Niemantsverdriet, J. W., van Grondelle, J., and van der Kraan, A. M., *Hyperfine Interact.* **28,** 867 (1986).
4. Niemantsverdriet, J. W., van Kaam, J. A. C., Flipse, C. F. J., and van der Kraan, A. M., *J. Catal.* **96,** 58 (1985).
5. Niemantsverdriet, J. W., van der Kraan, A. M., and Delgass, W. N., *J. Catal.* **89,** 138 (1984).
6. Niemantsverdriet, J. W., Aschenbeck, D. P., Fortunato, F. A., and Delgass, W. N., *J. Mol. Catal.* **25,** 285 (1984).
7. van't Blik, H. F. J., and Niemantsverdriet, J. W., *Appl. Catal.* **10,** 155 (1984).
8. Niemantsverdriet, J. W., van der Kraan, A. M., van Loef, J. J., and Delgass, W. N., *J. Phys. Chem.* **87,** 1292 (1983).
9. Minai, Y., Tominaga, T., Fukushima, T., and Ichikawa, M., *in* "Industrial Applications of the Mössbauer Effect" (G. J. Long and J. G. Stevens, Eds.), p. 635. Plenum, New York, 1986.
10. Minai, Y., Fukushima, T., Ichikawa, M., and Tominaga, T., *J. Radioanal. Nucl. Chem. Lett.* **87,** 189 (1984).
11. Lazar, K., Reiff, W. M., Mörke, W., and Guczi, L., *J. Catal.* **100,** 118 (1986).
12. Burton J. J. and Garten, R. L., *in* "Advanced Materials in Catalysis" (J. J. Burton and R. L. Garten, Eds.), Materials Science Series, p. 33. Academic Press, New York, 1977.
13. Garten, R. L., *in* "Mössbauer Effect Methodology" (I. J. Gruverman, Ed.), Vol. 10, p. 69. Plenum, New York, 1976.
14. Vannice, M. A., Lam, Y. L., and Garten, R. L., *Adv. Chem. Ser.* **178,** 25 (1979).
15. Berry, F. J., Liwu, L., Chengyu, W., Renyuan, T., Su, Z., and Dongbai, L., *J. Chem. Soc. Faraday Trans. 1* **81,** 2293 (1985).
16. Bartholomew, C. H., and Boudart, M., *J. Catal.* **29,** 278 (1973).
17. Gravelle, P. C., *Catal. Rev. Sci. Eng.* **16,** 37 (1977).
18. Gravelle, P. C., *Adv. Catal.* **22,** 191 (1972).
19. O'Neil, M., Lovrien, R., and Phillips, J., *Rev. Sci. Instrum.* **56,** 2312 (1985).
20. O'Neil, M., and Phillips, J., *J. Phys. Chem.* **91,** 2867 (1987).
21. Gatte, R. R., and Phillips, J., *Langmuir,* accepted for publication.
22. Gatte, R. R., and Phillips, J., "Proceedings, 43rd Calorimeter Conference, August 1988." *Thermochim. Acta,* in press.
23. Somorjai, G. A., "Chemistry in Two Dimensions: Surfaces." Cornell Univ. Press, Ithaca, NY, 1981.
24. Salzer, A., Egolf, T., and von Philipsborn, W., *Helv. Chim. Acta* **65,** 1145 (1982).
25. Shirane, G., Chen, C. W., Flinn, P. A., and Nathans, R., *J. Appl. Phys.* **34,** 1044 (1963).
26. Shirane, G., Chen, C. W., Flinn, P. A., and Nathans, R., *Phys. Rev.* **131,** 183 (1963).
27. Swartzendruber, L. J., *Bull. Alloy Phase Diagrams* **5,** 456 (1984).
28. Kubaschewski, O., *in* "Iron–Binary Phase Diagrams," p. 121. Springer-Verlag, West Berlin, 1982.
29. Matyi, R. J., Schwartz, L. H., and Butt, J. B., *Catal. Rev. Sci. Eng.* **29,** 41 (1987).
30. Kubaschewski, O., and Hopkins, B. E., *in* "Oxidation of Metals and Alloys," p. 114. Butterworths, London, 1967.
31. Wang, T., and Schmidt, L. D., *J. Catal.* **71,** 411 (1981).
32. Wang, T., and Schmidt, L. D., *J. Catal.* **70,** 187 (1981).
33. Chen, A. A., Vannice, M. A., and Phillips, J., *J. Catal.,* in press.
34. Wagner, C., *in* "Atom Movements," p. 153. Amer. Soc. for Metals, Cleveland, OH, 1951.
35. Brennan, D., Hayward, D. O., and Trapnell, B. M. W., *Proc. Soc. (London) Ser. A.* **256,** 81 (1960).
36. Langell, M., and Somorjai, G. A., *J. Vac. Sci. Technol.* **21,** 858 (1982).
37. Chakraborti, S., Datye, A. K., and Long, N. J., *J. Catal.* **108,** 444 (1987).
38. Wang, T., and Schmidt, L. D., *J. Catal.* **70,** 187 (1981).
39. Phillips, J., and Dumesic, J. A., *Appl. Catal.* **9,** 1 (1984).